BETTER SHIPS, BLUE OCEANS

NUMERICAL SIMULATIONS FOR AN OFFSHORE SEAWEED FARM - BLAUWWIND

Hydrodynamic Numerical Simulation

Text Report – Draft

Report No.	:	**34291-1-CPO**
Date	:	**November 2023**
Version	:	**1.0**

NUMERICAL SIMULATIONS FOR AN OFFSHORE SEAWEED FARM - BLAUWWIND

Hydrodynamic Numerical Simulation

Text Report – Draft

MARIN order No. : 34291

Number of pages : 31

Ordered by : Invest NL

Order document : BD2021020

Reported by : N. Baderiya and W. Otto
Reviewed by : F. Jaouen

Version	Date	Version description
1.0	November 2023	Draft report

CONTENTS PAGE

REVIEW OF TABLES AND FIGURES

Tables in the report:

Tables in the Table section:

Figures in the report:

Figures in the Figure section:

REVIEW OF DELIVERABLES

Report type		Content
Text report	MARIN report No. 34291-1-CPO	Present report

1 INTRODUCTION

1.1 Background

The North Sea Farmers is developing the first seaweed farm inside an offshore wind farm. The North Sea Farm #1 is an initiative joined by The Seaweed Company, Van Oord Marine Contractors, Algaia and is supported by InvestNL. MARIN is requested by InvestNL to perform independent numerical simulations on the mooring loads, in order to verify the study performed by Aqitec B.V. Main interest is the dynamic load in the Ultimate Limit State on a number of critical components. Two systems are considered, a simplified system mainly for model verification and the full system for design verification. FIGURE 1, FIGURE 2 and Figure 1-1 give an impression of the systems in question.

Figure 1-1: Impression of the full scale system

The present report is intended for internal use within the North Sea Farm #1 initiative and associated partners within the project. Besides the present report, a public conference paper is anticipated in which Aqitec B.V. and MARIN will present the lessons learned externally. The exact content of this public paper will be discussed in close cooperation with the consortium.

1.2 Objectives

The main objective of the project is as follows:

- To independently verify the loads simulated by the Aqitec
- To determine the dynamic load due to waves and current on a number of critical components

1.3 Content of the report

In this report the following topics are addressed:

- Description of the model used for the simulation campaign
- Interpretation of the results
- Conclusions

2 METHODOLOGY

2.1 Introduction

The time-domain simulation program aNySIM can simulate the behaviour of multiple (floating) bodies under the action of combined swell, wind seas, current and wind. More general information can be found in reference [1].

2.2 Morison Elements

Hydrodynamic loads on a mooring line, net or tube can be calculated by the Morison equation. The main assumption is that the object's cross section is small compared to the incoming wave length, such that the object does not significantly disturb (diffract) the incoming wave. For the seaweed farm this is a valid assumption. The Morison load is composed of three contributions.

$$F_{Morison} = F_{Froude-Krylov} + F_{Mass} + F_{Drag}$$

The Froude-Krylov component represents the surface integral of the undisturbed wave pressure on the object. According to Gauss theorem, this surface integral can be substituted by a more simple volume integral. Therefore the force equals the mass of the displaced water times the fluid acceleration of the undisturbed wave kinematics.

$$F_{Froude-Krylov} = \rho V \dot{u}_{fluid}$$

ρ	Density of (sea)water	[kg/m^3]
V	Fluid displaced by the body	[m^3]
$\dot{u}_{fluid}$	Fluid acceleration	[m/s^2]

For a circular cross-section with a finite length this volume is equal to:

$$V = (\pi/4) D^2 l$$

Where:

D	Diameter	[m]
l	Unit length	[m]

For the added mass component, the relative acceleration of the body with respect to the fluid is considered. The added mass force can be calculated with the following formula:

$$F_{Mass} = \rho (C_l - 1) V \left(\dot{u}_{fluid} - \dot{u}_{body} \right)$$

Where:

C_l	Added mass coefficient	[-]
$\dot{u}_{body}$	Acceleration of the body	[m/s^2]

The drag force is dependent on the relative velocity between the fluid and the structural member. For a one-dimensional flow the drag force is defined according to:

$$F_{Drag} = \frac{1}{2}\rho C_d A\left(u_{fluid} - u_{body}\right)\left|u_{fluid} - u_{body}\right|$$

Where:

C_d	Drag coefficient	[-]
A	Drag area	[m^2]
u_{fluid}	Fluid velocity	[m/s]
u_{body}	Velocity of the body	[m/s]

For a circular cross section the drag area of a finite element length (l) is equal to:

$$A = Dl$$

It should be noted that this formula is applied in the normal and tangential direction of the element. Tangent forces act parallel and normal forces perpendicular to the centreline of a Morison element. First, the fluid velocity is decomposed in the normal and tangential direction of the object. Then, the drag formula is applied in both directions separately, using a tangential $C_{d,t}$ and a normal $C_{d,n}$. Note, as a consequence the resulting drag is not necessarily in the direction of the incoming flow. The 'drag' also has a force component perpendicular to the incoming flow, effectively creating a lift. This is illustrated in the following example:

Table 2-1: Example of drag decomposition in normal and tangential, and the resulting lift

rho	1000	kg/m2
D	1	m
L	5	m
V	1	m/s
cd,t	1.4	[-]
cd,n	2.6	[-]

angle of attack	V tan	V nor	F tan	F nor	F total	Angle force wrt flow	Lift	Drag	Cl	Cd	C total
0	1.00	0.00	3500	0	3500	0	0	3500	0.0	1.4	1.40
30	0.87	0.50	2625	1625	3087	2	95	3086	0.0	1.2	1.23
60	0.50	0.87	875	4875	4953	20	1680	4659	0.7	1.9	1.98
90	0.00	1.00	0	6500	6500	0	0	6500	0.0	2.6	2.60

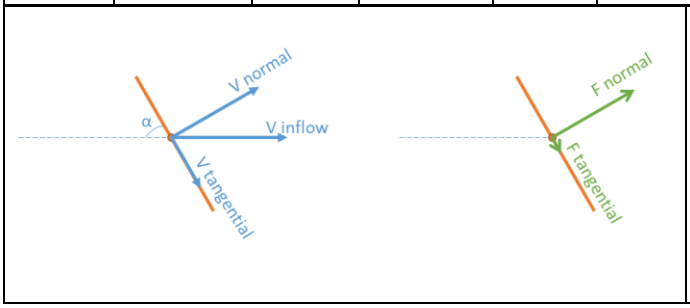

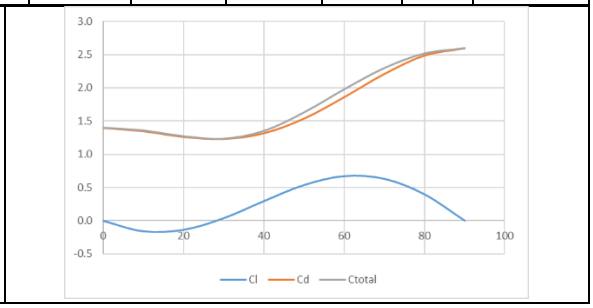

For partial submergence, i.e. when a Morison element is partially above water, the Froude-Krylov and added mass forces are based on the actual, instantaneous, submerged volume. The drag is based on

the instantaneous wetted area. Actual submerged volume and wetted area are computed each timestep based on the position of the object with respect to the waterline.

2.3 Wave kinematics

The Morison Elements rely on a description of the fluid velocity and acceleration. These wave kinematics are calculated with a first order non-viscous model, linearized in terms of wave height. The vertical fluid velocity u_z has a boundary condition at the seabed ($u_z = 0$) and at the waterline (u_z equals the velocity of the wave elevation). With a constant pressure assumed at the interface of air and water, the velocity potential for each wave component *i* becomes;

$$\Phi_i = -\frac{g a_i}{\omega_i} \frac{\cosh\big(k_i(z+h)\big)}{\cosh(k_i h)} \sin k_{ix} x + k_{iy} y - \omega_i t$$

Where a_i denotes the wave amplitude, g the gravity constant, h the water depth, ω the wave frequency and k the wave number given by the dispersion relation;

$$\omega_i{}^2 = g k_i \tanh k_i h$$

The fluid velocity follows naturally from the gradient of the potential function, and the fluid acceleration follows from the time derivative of the velocity.

As the described model is linearized in term of wave height, the wave kinematics are known from the seabed till the mean water level. In order to correct the model for the distance between the mean water level and the instantaneous wave elevation, Wheeler stretching [2] is applied. The velocity field is linearly stretched from the assumed still water line to the actual elevated water level.

This fist order model is computationally efficient and accurate for waves with a low steepness. For steeper waves, the model loses accuracy. Particularly in wave crests the fluid velocity is underestimated. Also, the wave height of this linear model follows a Rayleigh distribution, which underestimates the maximum wave height in an irregular sea state. These two effects may lead to non-conservative results. The model was chosen because it is similar to the to be verified simulations. Also, the additional cost of running a higher order model are substantial.

2.4 Mechanical interactions

The mooring lines, nets and tubes are discretised in a large number of rigid Morison Elements. These are connected to each other with mechanical joints. The joint stiffness in axial direction is derived based on the EA (Elasticity modulus and sectional Area) of the structure. In transverse and rotational direction the joint stiffness is chosen such that the discretised structure follows the bending deflection and rotation relations of an Euler beam, with the EI of the real structure. As all elements are cylindrical, only 5 degrees of freedom per element are solved. The rotation in tangential direction, which would create torsion, is not considered relevant and therefore not solved. The 5 solved degrees of freedom per discrete element are axial, shear in two directions and bending in two direction.

As the joints are stiff springs, solving the equation of motion directly in an explicit way would require very small timesteps. Therefore, the equation of motion is supplemented with constraint dynamics equations, which allows for an implicit way of solving the joint forces. With the implicit way, larger timesteps are feasible without numerical instabilities in the joints.

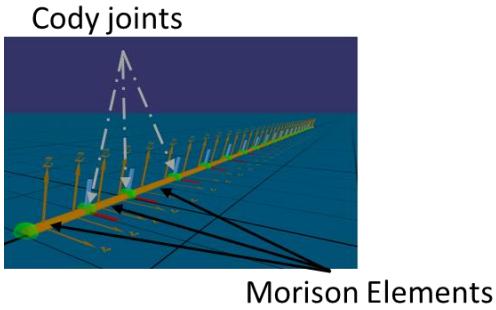

Figure 2-1: Visualisation of joints and elements

2.5 Seabed interaction

If an element is below the local waterdepth, we have seabed interaction. The seabed will apply a horizontal frictional force and a vertical restoring force to the element. The Coulomb friction force is computed based on the vertical downward component of the node force and the friction coefficient C_f. For low horizontal node velocities, the Coulomb friction is cut off at a friction slope for numerical stability. The slope is determined based on the outer loop time step and the dry node mass. The vertical load component and the vertical velocity of a node below the seabed are reset to zero. The z-coordinate is set at the local water depth.

2.6 Sign convention

The applied coordinate system is a right handed coordinate system with the Z-axis pointing upwards. In the simulations, the farm is parallel to the Y-axis of the coordinate system. This does not correspond to the orientation on the compass, see which is corrected for in Section 3.1.

The sign convention is shown in Figure 2-2. As can be seen, the environments with an incidence angle of 90 and 270 degrees are in-line with the farm. Waves with an incidence of 0 and 180 degrees are propagating perpendicular to the farm, i.e. the wave front and crests are parallel to the farm.

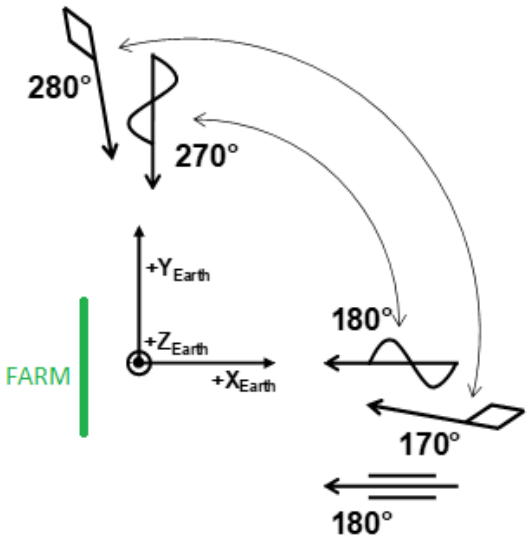

Figure 2-2: Coordinate system

3 INPUT PARAMETERS

3.1 Environmental conditions

The environmental conditions as given by Aqitec B.V. have been applied in this study. Only regular waves are defined. The wave height of the regular waves was chosen such that they correspond to the maximum wave height occurring in a certain irregular sea state. In this approach it is assumed that this largest wave event will result in the largest loading on the structure. As a cross-check, MARIN did compare the response in regular and irregular waves for one case.

The following sections give an overview of the environmental load cases of the simplified model and the full model respectively.

3.1.1 Simplified model

The load cases for the simplified model are tabulated on Table 3-1.

Table 3-1: Load cases for the simplified model

Load Case	Current speed [m/s]	Current Direction	Wave Height [m]	Wave Period [s]	Wave Direction
1	0	-	0	-	-
2	1	inline	0	-	-
3	1.2	inline	0	-	-
4	1	inline	4	8	inline
5	1	inline	4	8	perpendicular

3.1.2 Full model

In aNySIM-XMF the environmental direction is referenced as going towards as illustrated in Figure 2-2, which is opposite to the reference system taken by Aqitec (coming from direction)[2]. Therefore the necessary translation has been done to match the same direction as the Aqitec and is tabulated in Table 3-2.

Table 3-2: Load cases for the full model

Load Case	Current speed [m/s]	Current Direction [deg]	Wave Height [m]	Wave Period [s]	Wave Direction [deg]
1	1.0	225	14.12	10.74	315
2	1.0	45	14.69	12.50	195
3	0.67	15	14.12	10.74	315
4	1.56	285	14.12	10.74	225
5	1.56	285	13.95	10.45	255
6	1.43	285	14.12	10.74	315
7	1.52	105	14.12	10.74	225
8	1.52	105	13.95	10.45	255
9	1.17	105	13.95	10.45	285
10	1.17	105	14.12	10.74	315
11	1.56	270	13.95	10.45	270
12	0.67	180	14.69	12.50	180

For the avoidance of doubt, the wave and current directions relative to the farm are illustrated in Figure 3-1.

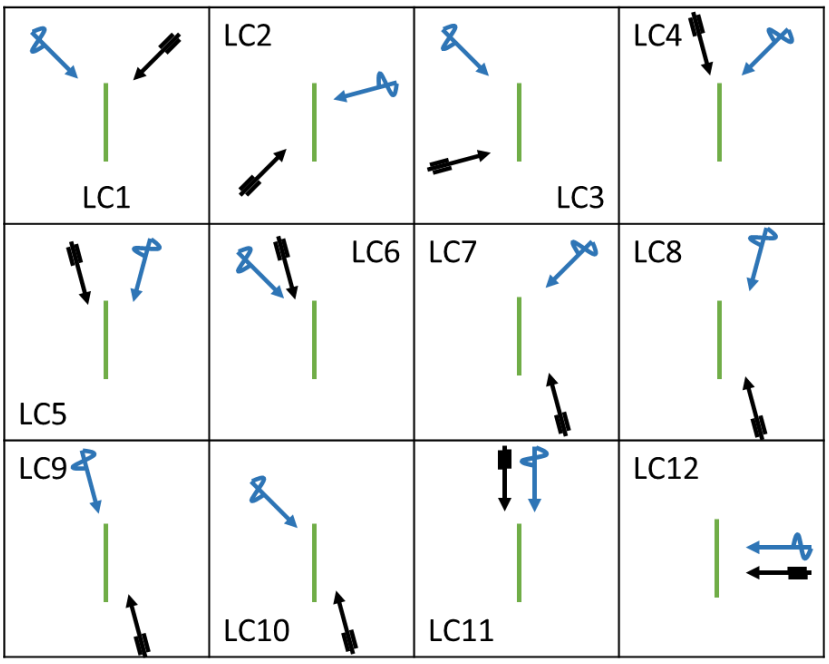

*Figure 3-1: Wave direction **(blue)**, current direction **(black)**, and seaweed farm **(green)***

3.2 Model setup

3.2.1 Simplified model

The simplified model is shown in Figure 3-2. The dimensions, structural properties and hydrodynamic coefficients as well as the numerical discretization of this model is given in TABLE 1. The element numbering in the figure below corresponds to the numbering in TABLE 1.

As a base case the hydrodynamic coefficients as applied by Aqitec have been used. MARIN has performed a sensitivity check to investigate the influence of hydrodynamic coefficients on the end result, i.e. the internal load in the structure.

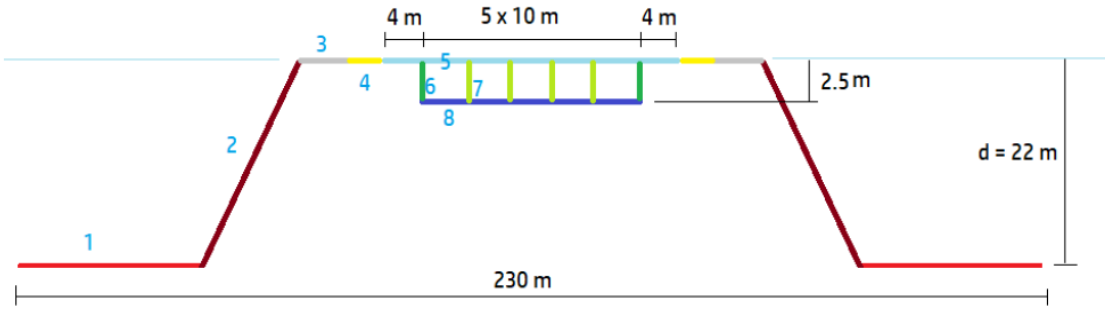

Figure 3-2: Schematic representation of the simplified model

3.2.2 Full model

The full model is shown in Figure 3-3. The dimensions, structural properties and hydrodynamic coefficients as well as the numerical discretization of this model is given in TABLE 2. The element numbering in the figure below corresponds to the numbering in TABLE 2.

Also here, as a base case the hydrodynamic coefficients as applied by Aqitec have been used. MARIN has performed a sensitivity check to investigate the influence of hydrodynamic coefficients on the end result, i.e. the internal load in the structure.

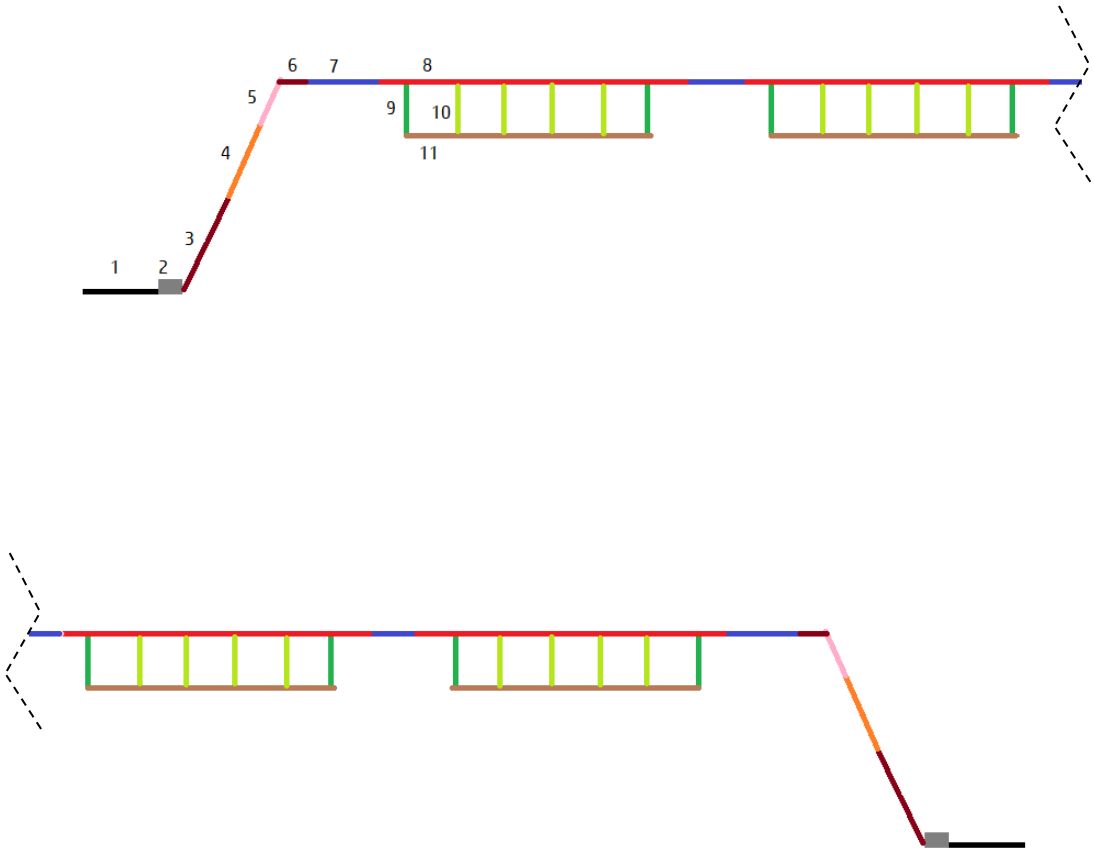

Figure 3-3: Schematic representation of the full model

4 SUMMARY OF THE RESULTS AND DISCUSSION

4.1 Simplified Model

The time traces of the force in the load link are shown in Figure 4-1, Figure 4-2 and Figure 4-3. The time traces are filtered to remove high frequency spurious oscillations due to the numerical solver.

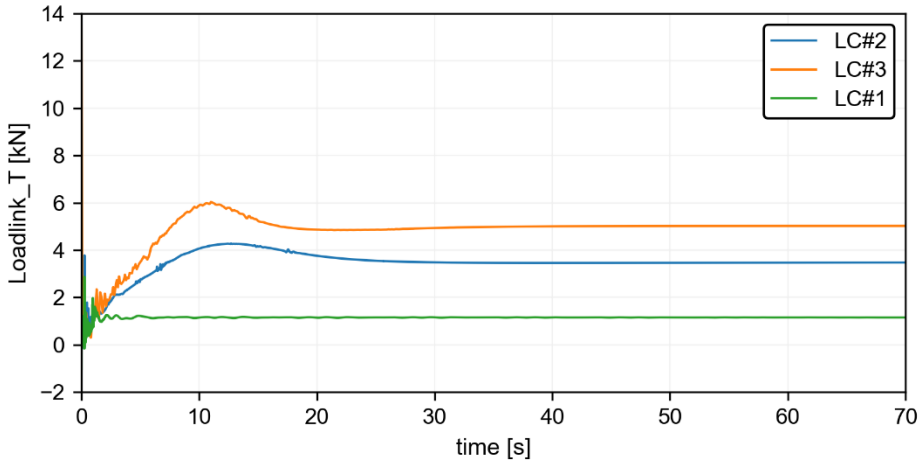

Figure 4-1: Loads for LC#1, LC#2 and LC#3

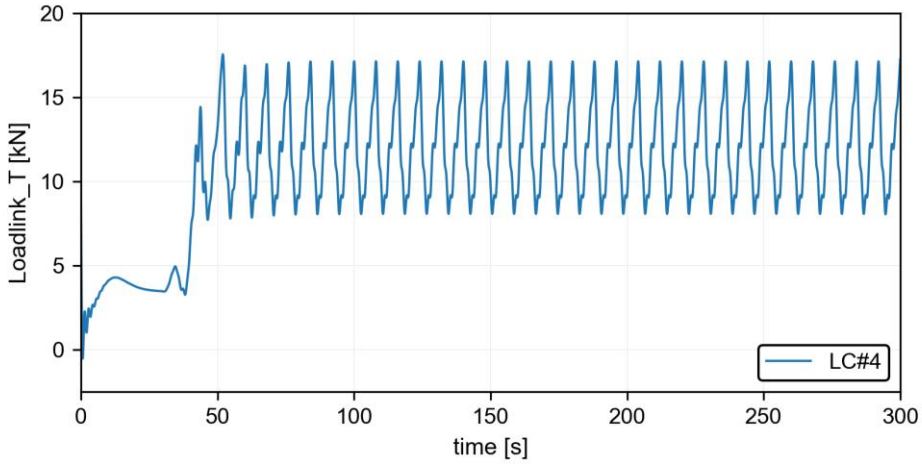

Figure 4-2: Loads for LC#4

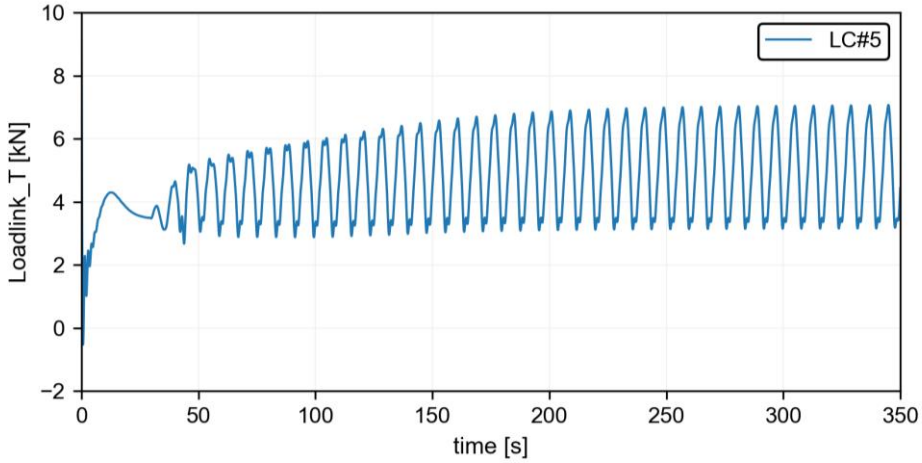

Figure 4-3: Loads for LC#5

The results are tabulated in Table 4-1. The reported maximum loads are determined from a section of the time trace where the results are stable (case 1 to 3), or become repetitive periodic (case 4&5).

Table 4-1: Results for the simplified model

Load Case	Current speed [m/s]	Current Direction	Wave Height [m]	Wave Period [s]	Wave Direction	Loads Load Link Aqitec [kN]	MARIN	
							Load in LoadLink [kN]	Difference [%]
1	0	-	0	-	-	1.2	1.2	1.7%
2	1.0	inline	0	-	-	4.3	3.5	19%
3	1.2	inline	0	-	-	5.9	5.0	15%
4	1.0	inline	4	8	inline	18.5	16.7	10%
5	1.0	inline	4	8	perpendicular	6.5	7.1	-9.1%

From load case 1 it can be seen that the still water equilibrium result is nearly identical to the to be verified results. For the current only cases the aNySIM XMF results are significantly lower than found at Aqitec. MARIN and Aqitec have discussed these results and performed several cross-checks to identify the source of this difference. From these discussions, it was identified that the most likely source is the in the partially submerged Morison elements. Hence for the elements which float in the waterline, part of the objects surface does not make contact with water. In aNySIM XMF the drag is determined based on the instantaneous wetted surface, while at Aqitec the drag is based on the complete surface area. This makes the results of Aqitec more conservative.

For the critical load case 4, which leads to the highest load in the load link, aNySIM XMF predicts a 10% lower load, most likely due to the treatment of the partial submergence.

The obtained difference in load case 5 cannot easily be explained. Percentage wise it is a significant difference. As this case is not critical for the design and the absolute difference is small, the difference is deemed acceptable.

4.1.1 Drag sensitivity analysis

It should be noted that there is a large uncertainty in the drag coefficient. The uncertainty is partially due to a lack of full scale experimental data, hence this will be the first large offshore seaweed farm. The uncertainty is also due to the organic nature of the farm, the quantity and quality of the product produced varies over time and is influenced by many parameters. Hence, the assumed drag coefficient can easily be significantly under or over estimated.

Therefore a sensitivity analysis on the drag coefficient is performed to see the impact of it on the loads of the load link. The simulations of load case 4 and 5 have been repeated with a 10% increased drag coefficients of the floats and nets. Note, the 10% is chosen as an example, the uncertainty is not necessarily limited to 10%. The results are tabulated in Table 4-2 and plotted in Figure 4-4 and Figure 4-5.

Table 4-2: Results for the sensitivity study

Load Case	With original drag	With 10% increased drag	Difference [%]
	Loads in LoadLink [kN]		
4	16.7	17.2	2.91%
5	7.1	8.2	13.41%

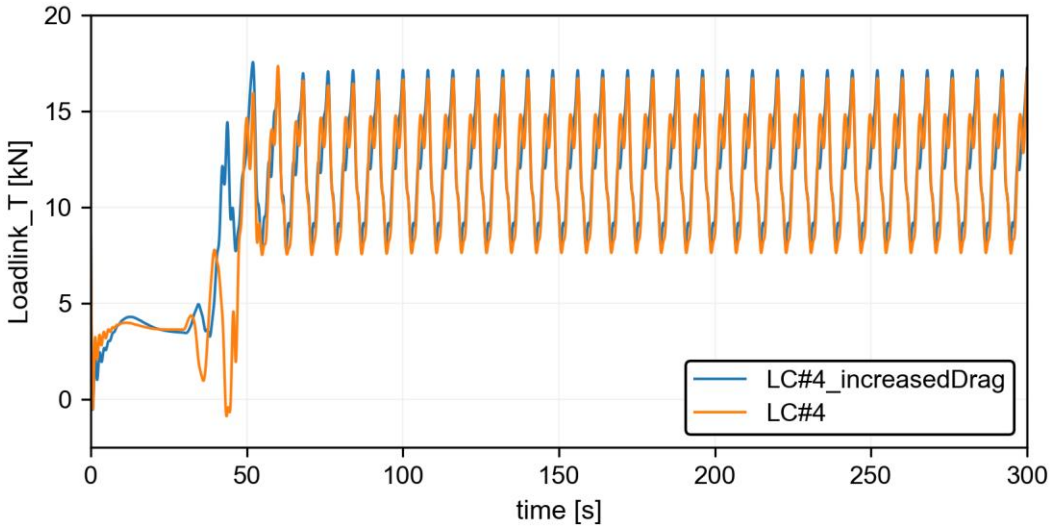

Figure 4-4: Drag sensitivity study for LC#4

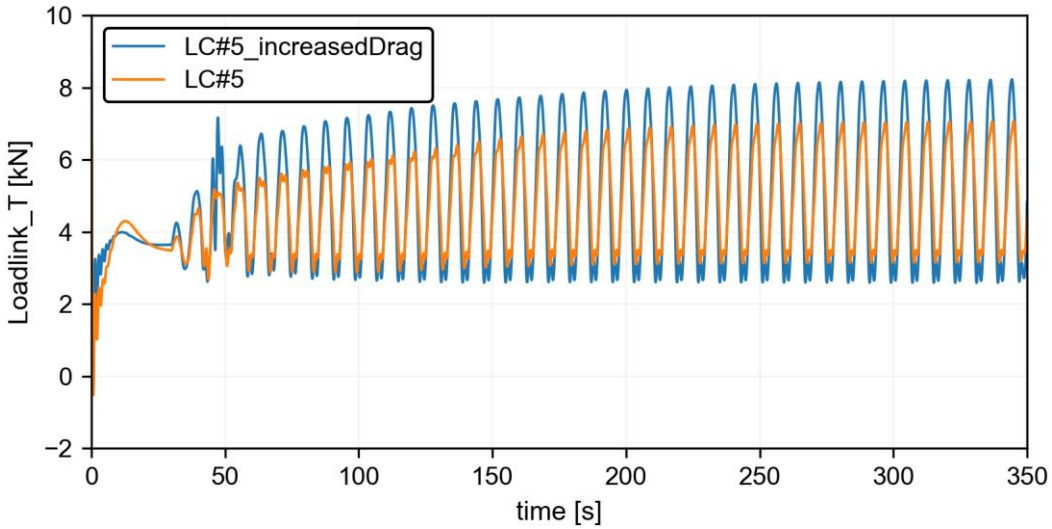

Figure 4-5: Drag sensitivity study for LC#5

For the critical load case 4, it can be seen that a 10% increase in drag coefficient only leads to 2.9% increase in loads in the load link. As the drag coefficient is an uncertain input parameter, it is favourable that the end result, i.e. the load in the load link, is not too sensitive to this parameter.

For the less critical load case 5, a 10% increase in drag coefficient leads to 13% higher loads at the load link.

4.2 Full Model

4.2.1 Regular wave results

Similar to the post-processing in the simplified model, the load time traces are filtered to remove high frequency spurious oscillations due to the numerical solver. The reported maximum loads are determined from a section of the time trace where the results become repetitive and periodic. The maximum loads at various locations are reported in Table 4-3. The locations are labelled in FIGURE 3.

Table 4-3: Maximum load [kN] in 12 load cases at various components

			*	*	*	*	*	*			*	*
Loadcase	1	2	3	4	5	6	7	8	9	10	11	12
Fair Front	80	91	262	89	97	177	262	313	123	107	103	424
Fair Aft	193	54	285	370	382	475	129	80	81	107	400	419
Anchor Front	36	98	242	0	0	139	258	307	116	104	0	408
anchor Aft	179	40	274	361	380	468	111	57	42	20	395	402
F6front_F7front	51	74	243	73	95	147	249	300	99	87	83	428
F7aft_F6aft	192	28	289	374	390	480	111	74	39	14	390	417
F7front_F8net1	51	74	243	71	93	147	250	300	100	88	84	429
F8net4_F7aft	192	31	288	374	390	482	111	74	39	15	390	417
F8net1_F7part1	133	40	254	200	212	280	247	149	67	70	222	414
F8net2_F7part2	153	46	295	253	265	298	252	181	68	58	272	402
F8net3_F7part3	154	37	245	264	384	372	241	151	74	37	408	405
F7part1_F8net2	133	40	254	200	212	280	247	149	69	71	222	413
F7part2_F8net3	153	45	296	250	263	297	252	179	68	58	272	404
F7part3_F8net4	154	37	244	264	383	372	240	151	74	37	408	405
Net1	32	16	11	45	63	36	15	38	49	25	69	17
Net2	24	6	24	42	72	58	23	42	32	12	78	15
Net3	24	5	38	51	69	61	30	48	30	20	72	13
Net4	25	6	35	38	44	41	44	32	23	8	48	15

** in these cases there is uplift of the chain at the anchor*

The highest occurring load is 485 kN, logged in load case 6. In general, the load cases where waves and current are (near) collinear result in the highest loads. The load cases where current and waves are in (near) opposed direction generally lead to lower load levels.

In a number of load cases there is uplift of the chain at the anchor. These are marked with an asterisk *. The uplift events do not lead to a sharp increase in tension. However, it is recommended to select anchors which allow for uplift.

4.2.2 Regular and Irregular wave

The regular wave approach assumes that the highest load in an irregular sea is similar to a load in a regular wave with a height corresponding to the highest wave of the irregular sea. To verify this assumption, an irregular wave is simulated for load case 11, which is collinear waves and current, in-line with the farm.

The resulting fairlead tension is shown in Figure 4-6 and Figure 4-7. Note, the regular wave is started after 300 seconds. From the probability of exceedance of the wave elevation, it can be seen that the irregular time trace contains two wave events with similar elevation as the regular wave. The maximum tension in the regular wave simulations is 400 kN, compared to 372 kN in the irregular wave.

It is difficult to draw generalized conclusions out of this specific case, however it is a good indication that the regular wave approach gives results representative for the maximum events in an irregular wave simulation.

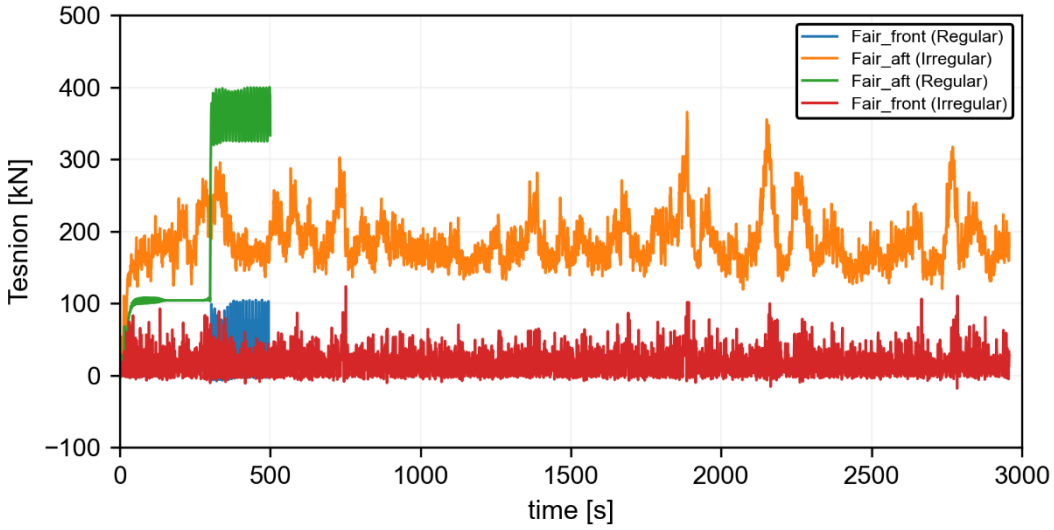

Figure 4-6: Tension time trace in an irregular sea state

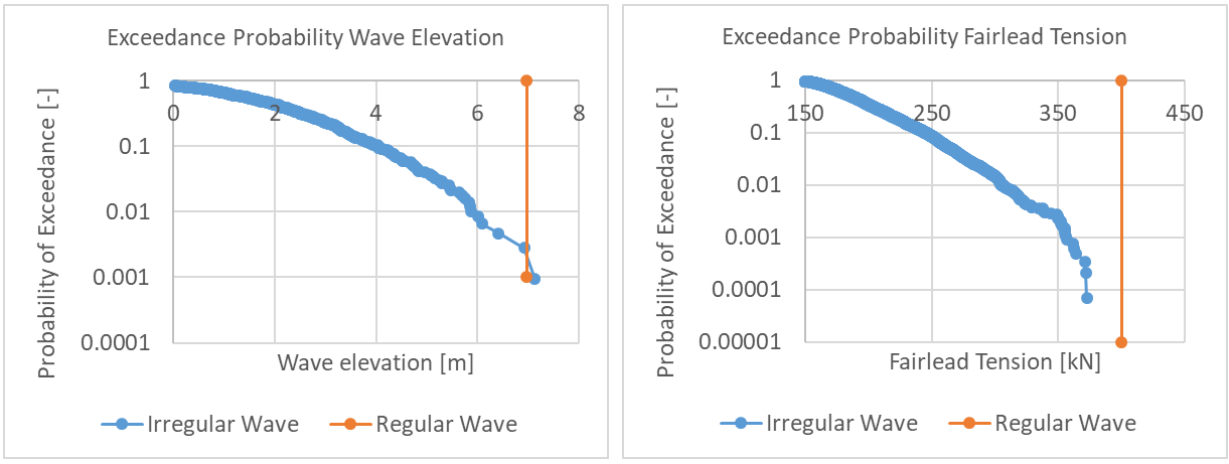

Figure 4-7: Probability of exceedance

The chain uplift at the anchor location is plotted in Figure 4-8, in which a Z level of -35m corresponds to the seabed. It can be seen that chain uplift occurs in the regular waves as well as in the irregular waves. The uplift is not an artefact of the regular wave approach.

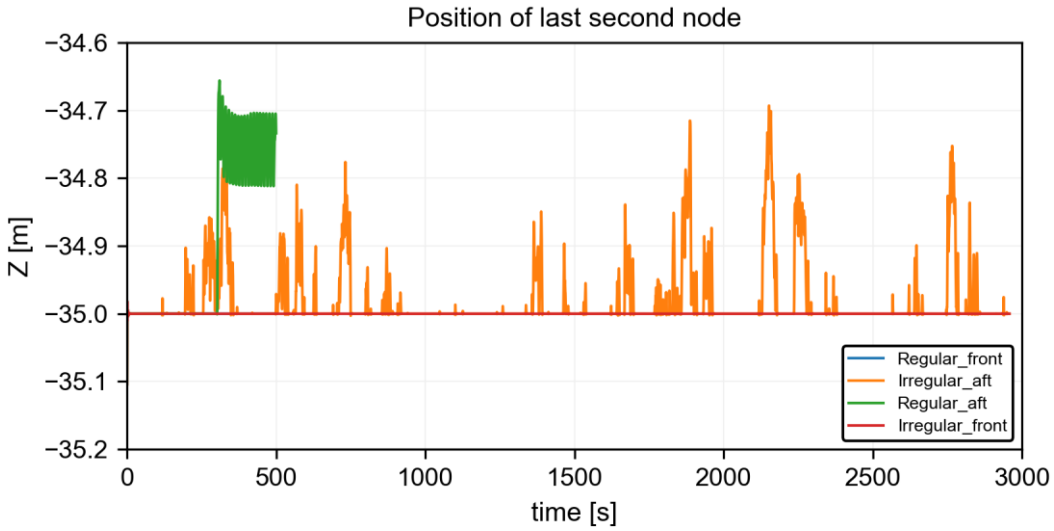

Figure 4-8: Position of last second node of mooring lines

5 CONCLUSIONS AND RECOMMENDATIONS

Hydrodynamic simulations are performed based on a Morison approach with wave kinematics derived from a linear potential model. Simulations with a simplified farm lay-out have been performed in software aNySIM-XMF in order to independently verify the numerical simulations performed at Aqitec.

- The still water equilibrium result is nearly identical to the to be verified results.
- For the current only cases the aNySIM XMF results are significantly lower than found at Aqitec. In 1.2 m/s current, the aNySIM- XMF results are 15% lower.
- MARIN and Aqitec have discussed these results and performed several cross-checks to identify the source of this difference. From these discussions, it was identified that the most likely source is how the two simulations handle with partially submerged objects. The way these are treated by Aqitec can be considered as conservative.
- For the critical load case 4, being wave and current in-line with the farm, aNySIM XMF predicts a 10% lower load than Aqitec. This is also most likely due to the treatment of the partial submergence.
- The obtained difference in load case 5 cannot easily be explained. This is in waves and current perpendicular to the farm. Although percentage wise there is a significant difference, this is not a critical load case and the absolute difference is small. Therefore the difference is deemed acceptable.
- The drag coefficient is an input parameter with a large uncertainty. Therefore two load cases were repeated with a 10% increased drag coefficient as a sensitivity check. Note, the 10% is chosen as an example, the uncertainty is not necessarily limited to 10%. For the critical load case 4, the increased drag only leads to 2.9% increase in dynamic maximum loads. For the non-critical load case 5, the increased drag increases dynamic maximum load with 13%.

Simulations with the full farm lay-out have been performed

- The highest occurring load is 485 kN, which occurs at the fairlead and is logged in load case 6. In general, load cases where waves and current are (near) collinear result in the highest loads. Load cases where current and waves are in (near) opposed direction generally lead to lower load levels.
- In a number of load cases there is uplift of the chain at the anchor. The uplift events do not lead to a sharp increase in tension. It is recommended to select anchors which allow for uplift.
- The regular wave approach assumes that the highest load in an irregular sea is similar to a load in a regular wave with a height corresponding to the highest wave of the irregular sea. To verify this assumption, an irregular wave is simulated for load case 11, which is collinear waves and current, in-line with the full farm. The maximum tension in the regular wave simulations is 400 kN, compared to 372 kN in the irregular wave. It is difficult to draw generalized conclusions out of this specific case, however it is a good indication that the regular wave approach gives results representative for the maximum events in an irregular wave simulation.

Compared to higher order models, the linear wave kinematic model underestimates the maximum fluid velocity in the wave crest, and underestimates the ultimate crest height. These two effects may lead to non-conservative results. Higher order simulations will be able to reduce the modelling errors, however the cost of such simulations are substantial. Alternatively the uncertainties can be reduced by monitoring the full scale pilot. This is probably the most cost effective way, under the condition that the safety of personnel and environment are not at risk should a failure occur.

Wageningen, November 2023
MARITIME RESEARCH INSTITUTE NETHERLANDS

Ir. O.J. Waals
Manager Offshore

REFERENCES

[1] https://www.marin.nl/en/publications/anysim-a-versatile-hydrodynamics-engineering-tool

[2] Wheeler J.D. (1970), “Method for calculating forces produced by irregular waves”, Journal of Petroleum Technology, Vol. 22, No. 3, pp. 359-367

[3] NSF#1: Full model characterization

TABLES

TABLE 1 SIMPLIFIED MODEL

#	Length [m]	Type	E-mod [Mpa]	Diameter [mm]	Fouling thickness [mm]	Weight [kg/m]	Weight incl. fouling [kg/m]	MBL [kN]	Relative density	Subm weight [N/m]	Dry weight [N/m]	Cf [static/dynamic]	Segmented in n beam elements	Cd [perp]	Cd [parallel]	Ca [perp/parallel]
1	41	Studlink chain	128000	48	0	51	51	1196	7.8	436	500	0.98 / 0.75	6	2.6	1	1 / 0.5
2	51	Studlink chain	128000	19	20	7.9	*14.3*	445	7.8	80.8	140	0.98 / 0.75	10	2.6	1	1 / 0.5
3A	*2.5*	*Horizontal floater - structural component*	*128000*	*19*	*0*	*7.9*	*7.9*	*445*	*7.8*	67.6	77.5	-	-	*2.6*	*1*	*1 / 0.5*
3B	*2.5*	*Horizontal floater - floater*	-	*550*	*20*	*22.5*	*69.1*	-	*0.11*	-1689	677	-	-	*0.6*	*0.1*	*1 / 0.5*
3	2.5	Horizontal floater - total	128000		-	30.4	77.0	445	-	-1621	755	-	3			1 / 0.5
4	2	Loadlinks & Shackles	128000	48	20	15.5	*26.6*	508	7.8	156	261	-	2	2.6		1 / 0.5
5A		*Horizontal floater - structural component*	*1400*	*44*	*0*	*0.9*	*0.9*	*280*	*0.93*	-0.66	8.83	-	-	*1.8*	*1*	*1 / 0.5*
5B		*Horizontal floater - floater*	-	*250*	*0*	*8.3*	*8.3*	-	*0.17*	-397.5	81.4	-	-	*1.17*	*0*	*1 / 0.5*
5	58	Horizontal floater - total	1400	250	0	9.2	9.2	280	-	-398.2	90.3	-	2 / 3 / 3 / 3 / 3 / 3 / 2			1 / 0.5
														1.8	1	
5*		*Horizontal floater first and last element*	-		0	9.2	9.2	280			90.3				*0*	1 / 0.5
6	2.5	Net - Outside	1600	49	0	22	22	164	1	0.0	215	-	4	0.22	0.04	1 / 0.5
7	2.5	Net - Inside	1600	64	0	44	44	326	1	0.0	431	-	4	0.22	0.04	1 / 0.5
8	50	Hercules rope	50000	18	0	0.47	0.47	79	1.85	2.1	4.61	-	3 / 3 / 3 / 3 / 3	1.8	0	1 / 0.5

TABLE 2 FULL MODEL

#	Length [m]	Type	E-mod [Mpa]	Diameter [mm]	Fouling thickness [mm]	Weight [kg/m]	Weight incl. fouling [kg/m]	MBL / SWL [kN]	Relative density	Subm weight [N/m]	Dry weight [N/m]	Cf [static / dynamic]	Segmented in n beam elements	Cd perpend	Cd parallel	Ca [perp / parallel]
1	53	Stud link chain	128000	58	0	77	*77*	2953 / 879	7.8	659	755	0.98 / 0.75	12	2.6	1	1 / 0.5
2	2	Clump weight + chain	128000	58	50	792	*857*	2953 / 879	2.57	4882	8410	1 / 0.75	3	2.6	1	0.5 / 0.5
3	19	Stud link chain	128000	48	50	52.8	*93*	2063 / 842	7.8	535	911	0.98 / 0.75	5	2.6	1	1 / 0.5
4	23	Dyneema – Low fouling	50000	56	50	1.74	*23*	2490 / 866	0.98	45	229	-	7	0.6	0.1	1 / 0.5
5	7	Dyneema – High fouling	50000	56	150	1.74	*128*	2490 / 866	0.98	262	1255	-	2	0	0	1 / 0.5
6A		Horizontal Floater – Structural Component	50000	56	0	1.74	*1.7*	2490 / 866	0.98	-0.35	17.1	-	-	0	0	1 / 0.5
6B		Horizontal Floater – Buoyancy	-	1000	150	235	*940*	-	0.3	-3917	9217	-	-	0.6	0.32	0.6 / 0.6
6	3	Horizontal Floater	-	-	-		*941*			*-3917*	*9234*	-	3			-
7	13 / 6 / 6 /6 /13	Mooring Rope	1400	112	20	5.96	*16.7*	1870 / 650	0.93	18.0	164	-	4 / 3 / 3/ 3 / 4 [3.25 m / 2 m]			1 / 0.5
	13	Mooring Rope	1400	112	20	5.96	*16.7*	1870 / 650	0.93	18.0	164	-	4	1.8	0	
	6	Mooring Rope	1400	112	20	5.96	*16.7*	1870 / 650	0.93	18.0	164	-	3	1.8	0	
8A		Horizontal Floater – Structural Component (rope)	1400	112	20	5.96	*16.7*	1870 / 650	0.93	18.0	164	-	-	1.8	0	1 / 0.5
8B		Horizontal Floater – Buoyancy	-	250	0	8.3	*8.3*	-	0.17	-398	81.4	-	-	1.17	0	1 / 0.5
8	4 x -- 2/10/10/10/10/10/2	Horizontal Floater	-	-	-	14.26	*25.0*			-380	246	-	4x -- 3/3/3/3/3/3/3			-
	2	Horizontal Floater				14.26	*25.0*			-380	246		3			
	10	Horizontal Floater				14.26	*25.0*			-380	246		3			
9	3.5	Net - Outside	1600	49	0	43	*43.0*	378 / 263	1.025	10.3	422	-	4			1 / 0.5
10	3.5	Net – Inside	1600	64	0	86	*86.0*	651 / 453	1.025	20.6	844	-	4			1 / 0.5
11	4x -- 10/10/10/10	Hercules rope	50000	24	0	0.98	*0.98*	174 / 121	1.85	4.4	9.6	-	3 / 3 / 3 / 3 / 3			1 / 0.5
	10	Hercules rope	50000	24	0	0.98	*0.98*	174 / 121	1.85	4.4	9.6		3			

FIGURES

FIGURE 1 SIMPLIFIED MODEL

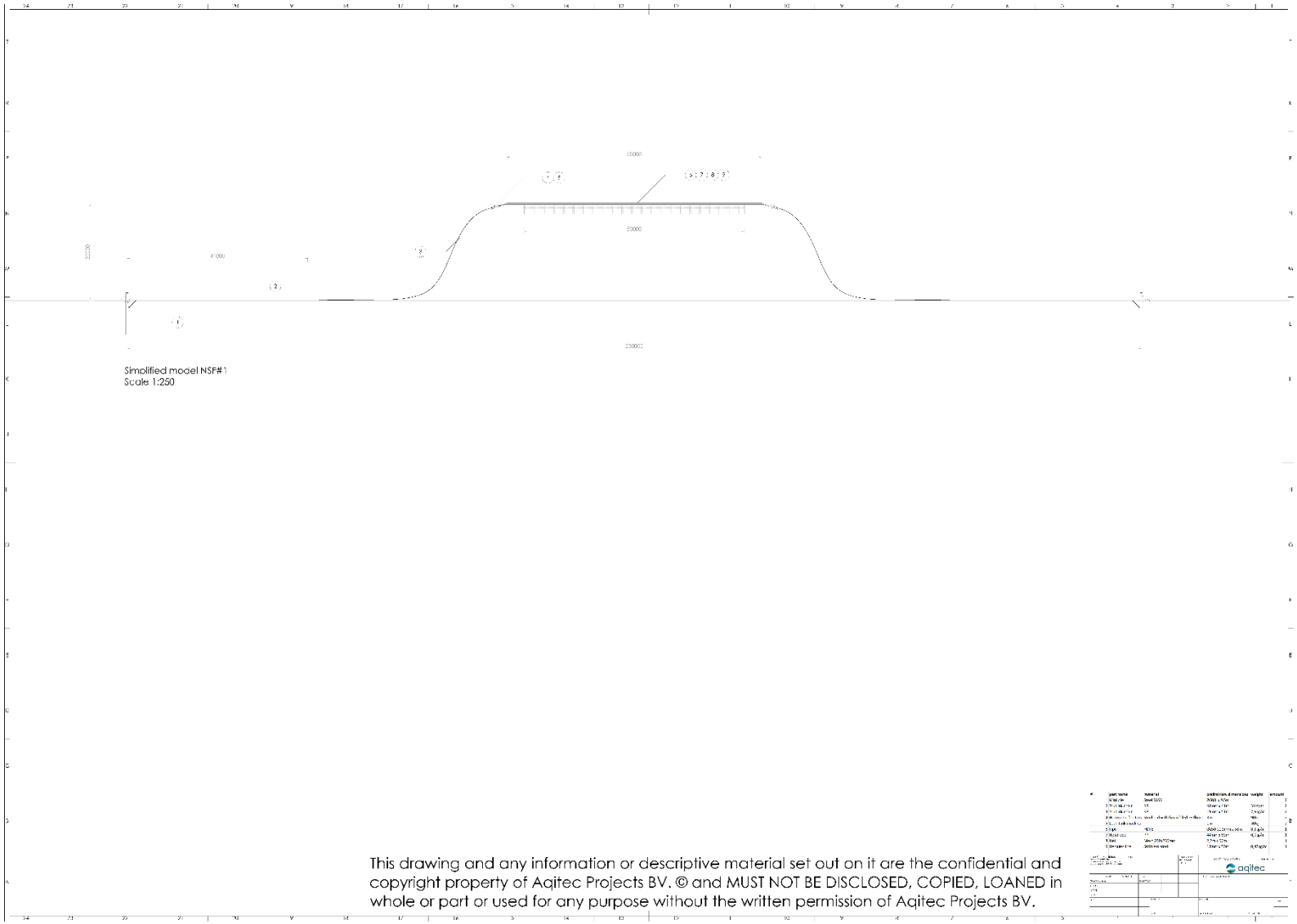

FIGURE 2 FULL MODEL

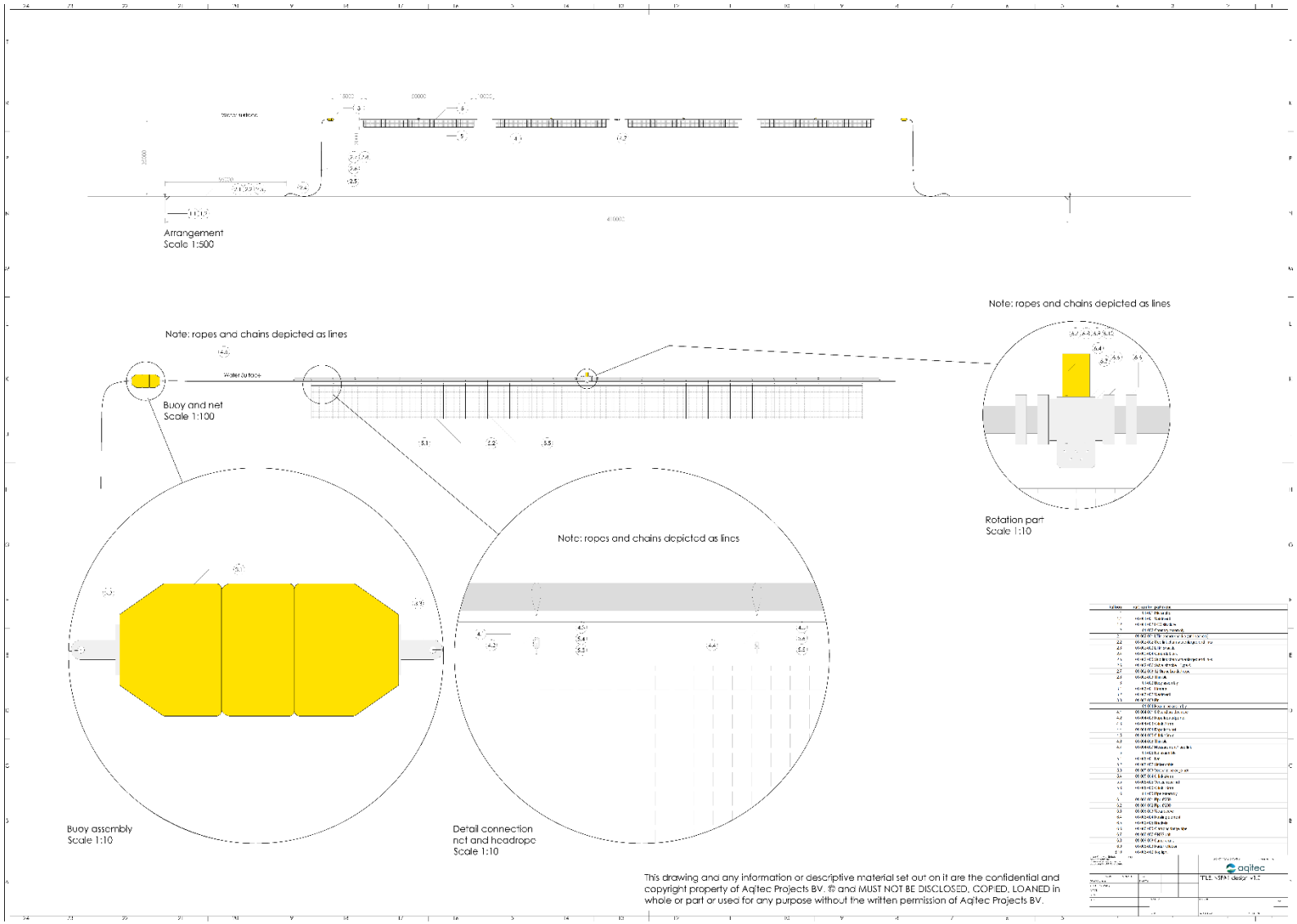

FIGURE 3 FULL MODEL INCLUDING LOCATIONS OF FORCE MEASUREMENT

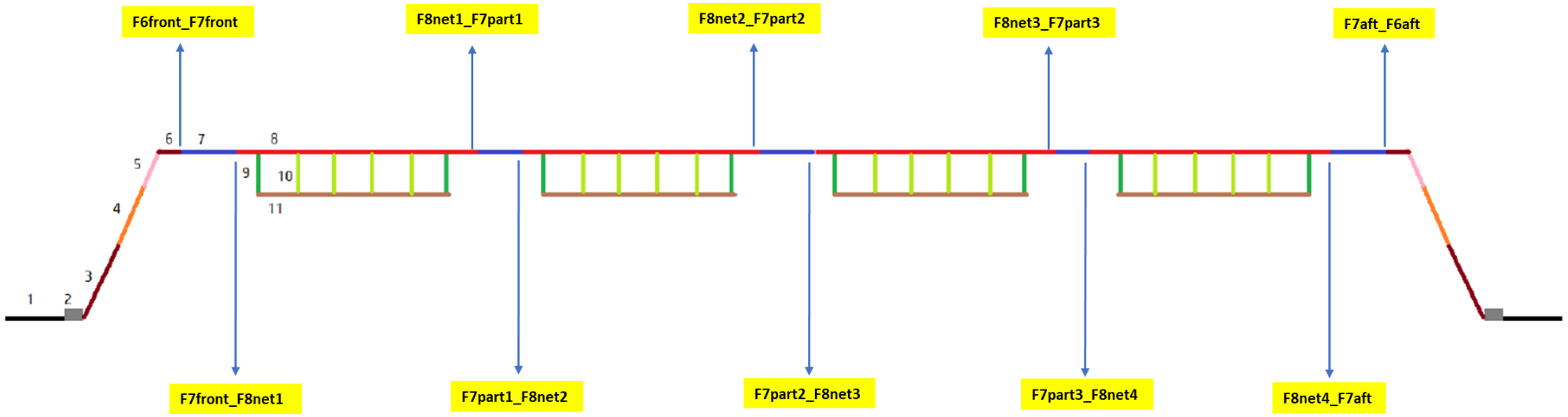

M A R I N
P.O. Box 28

6700 AA Wageningen
The Netherlands

T +31 317 49 39 11
E info@marin.nl

I www.marin.nl